Geopersia ***5*** *(2), 2015, PP. 93- 109*

Source and diagenesis of Middle Jurassic marine mudstones, Kopet-Dagh Basin, NE Iran

Mehdi Reza Poursoltani[1]*, Georgia Pe-Piper[2]
[1] *Department of Geology, Mashhad Branch, Islamic Azad University, Mashhad, Iran*
[2] *Department of Geology, Saint Mary's University, Halifax, Nova Scotia, Canada B3H 3C3*
**Corresponding author, e-mail: poursoltani1852@mshdiau.ac.ir*
(*received: 05/06/2015 ; accepted: 25/11/2015*)

Abstract

Middle Jurassic fluvio-deltaic and turbiditic mudstones of the Kashafrud Formation are important hydrocarbon sources in the gas-rich Kopet-Dagh Basin, northeastern Iran. Clay mineral assemblages are important for the interpretation of sediment provenance and for understanding burial diagenetic cementation in sandstones. The clay mineral assemblages in fluvio-deltaic and turbiditic mudrocks in two areas, Saleh-Abad and Senjedak, were investigated by X-ray diffraction analysis. A total of 28 bulk samples (half of which were taken from Saleh-Abad and the other half from Senjedak) were analysed and from 11 of these samples the <2 µm fraction was separated and analysed. The clay minerals identified are mostly kaolinite, illite, muscovite, chlorite, mixed-layer illite-chlorite, and very rarely smectite. Clay mineral assemblages result partly from variable detrital supply and partly from burial diagenesis. Detrital muscovite is more abundant at higher stratigraphic levels. Detrital smectite was rare; the lack of detectable illite-smectite mixed layer clays indicates that low smectite abundance is not the result of illitization. Vitrinite reflectance suggests burial to depths of only 2–3 km. Burial diagenesis resulted in more chlorite and more ordered mixed-layer chlorite-illite at greater burial depths. The source area for the basin was a rapidly rising area that included illitic shales, overlying crystalline basement of granite, and low-grade metamorphic rocks, which supplied muscovite and chlorite.

Keywords: *Burial Diagenesis, Clay Minerals, Middle Jurassic, Kopet-Dagh Basin, Iran.*

Introduction

The Mesozoic Kopet-Dagh Basin, northeast Iran, is an important petroleum basin that hosts the giant Khangiran and Gonbadli gas fields (Kavoosi *et al.*, 2009). The Middle Jurassic Kashafrud Formation contains some of the hydrocarbon source rocks (Afshar Harb, 1979; Poursoltani & Gibling, 2011). The formation has been interpreted as a fluvio-deltaic and turbiditic formation (Afshar Harb, 1979; Madani, 1977; Poursoltani *et al.*, 2007a; Taheri *et al.*, 2009; Poursoltani & Kargar, 2012). The diagenetic cements in the sandstones of the Kashafrud Formation are of decisive importance in determining the reservoir quality (Poursoltani & Gibling, 2011). Poursoltani and Gibling (2011) used vitrinite reflectance to determine the degree of hydrocarbon maturation in the basin. Since most studies of the Kashafrud Formation have focused on paleoenvironments and sedimentology (Madani, 1977; Poursoltani *et al.*, 2007a), ichnology (Madani, 1977; Poursoltani *et al.*, 2007b; Taheri *et al.*, 2009), and lithological description (Poursoltani & Gibling, 2011), no detailed investigation of the role of clay mineral burial has been attempted.

Clay mineral assemblages in mudstones are important for understanding the history of burial diagenesis (*e.g.* Worden & Morad, 2003). For example, conversion of smectite to illite releases water and acts as a sink for the K released by the dissolution of feldspar in sandstones. Variations in clay minerals due to diagenesis must be understood if the provenance significance of clay minerals is to be interpreted. The aim of this study is to document and interpret the stratigraphic distribution of clay minerals in the Kashafrud Formation to identify the diagenetic influences and potential provenance.

Geological setting

The post-Paleozoic history of northeastern Iran and the stratigraphy and sedimentology of the Kashafrud Formation were outlined by Poursoltani *et al.* (2007a). Following the early Mesozoic closure of the Paleo-Tethys Ocean (Golonka, 2004), mid Jurassic sedimentation commenced in the Kopet-Dagh Basin, where 7 km of post-Triassic strata accumulated (Moussavi-Harami and Brenner, 1992; Aghanabati, 2004). The Kopet-Dagh Basin extends 700 km along strike, and the basin fill thickens southwards over 200 km from southern Turkmenistan to northeastern Iran, with zones of abrupt thickening that are inferred to mark extensional faults (Lyberis & Manby, 1999; Thomas *et al.*, 1999a, b). The basin experienced maximum subsidence in the Jurassic, when many

areas were underfilled and accumulated deep-water sediments of the Kashafrud and Chaman Bid formations.

The Kashafrud Formation is Middle Jurassic (Upper Bajocian-Lower Bathonian) in age, and rests nonconformably on ultramafic rocks in the study area (Fig. 1). The formation covers a large tract in northeast Iran, and was studied in two areas where its base and top are observed: at Senjedak, where it is 1200 m thick, and at Saleh-Abad (1753 m thick). The Kashafrud Formation is disconformably overlain by marine carbonates and evaporites of the Mozduran Formation (Oxfordian to Kimmeridgian), locally as much as 420 m thick (Lassemi, 1995; Kavoosi *et al.*, 2009).

The Kashafrud Formation comprises of 12 facies, which were assigned facies codes commencing with G, S, M, and C, respectively (Table 1, Poursoltani *et al.*, 2007a; Poursoltani & Kargar, 2012). These facies are grouped into two facies associations. The basal Conglomerate Facies Association consists of fluvio-marine conglomerates laid down as fan-delta deposits.

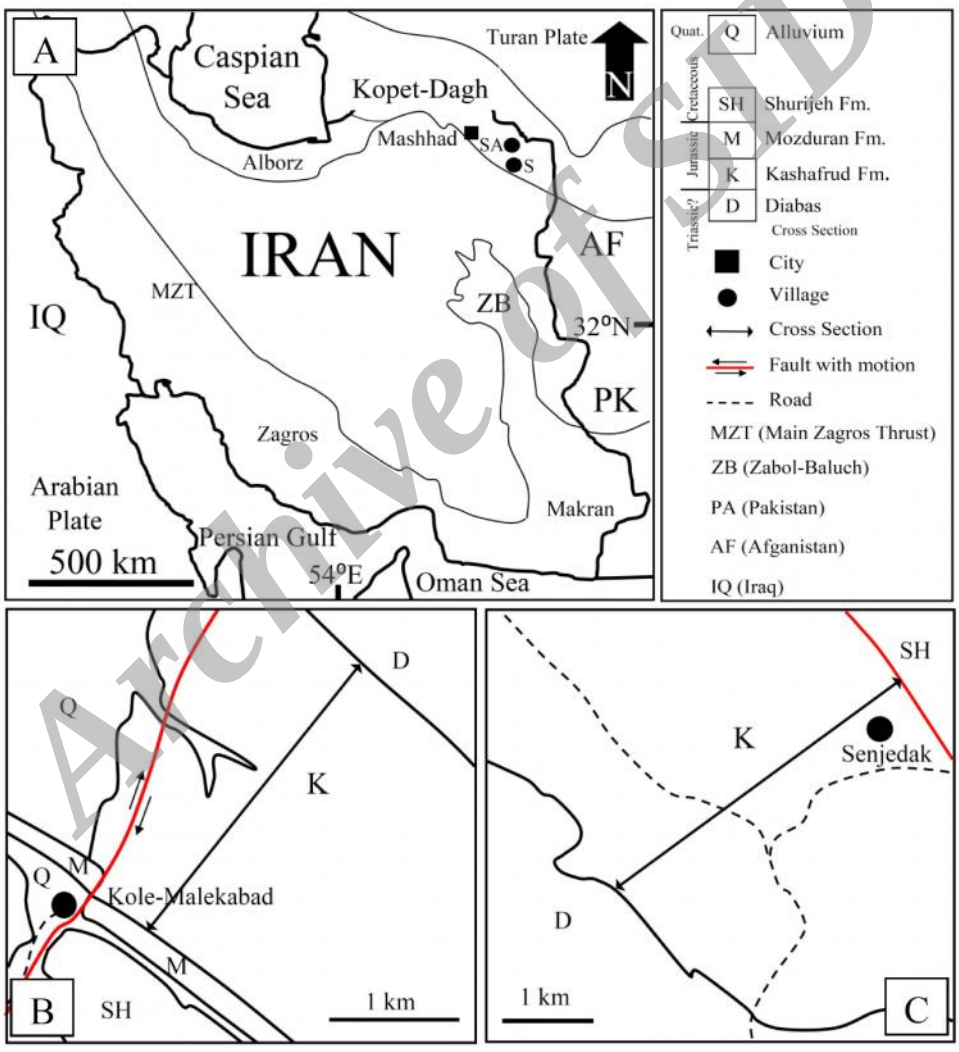

Figure 1. A) Map showing the location of Iran and the study areas in the Kopet-Dagh Basin of northeast Iran. The geological maps show the location of the two studied sections: B) Saleh-Abad (SA), C) Senjedak (S). Simplified from Iran Geological Survey map sheets Agh-Darband (Ghaemi, 2004) and Torbate-Jam (Eftekhar Nejad, *et al.*, 1993). Alborz and Kopet-Dagh show locations of mountainous areas referred to in the text. The North Afghan Platform lies in Afghanistan, east of the Torbate-Jam area of Iran.

Table 1. Facies distinguished in the Kashafrud Formation (Simplified from Poursoltani *et al.*, 2007a)

Facies	Sedimentary features	Depositional Conditions
G: Conglomerate		
(Gms) Matrix-supported conglomerate	Monomictic conglomerate in units up to 10 m thick. Clasts < 50 cm diameter, well-rounded to subrounded, well sorted to poorly sorted. Clasts show little preferred orientation, some beds imbricated, normal grading rarely present. Rests on flat-lying to concave-up erosion surface. Internal erosion surfaces in some units.	Cohesive debris flows to hyperconcentrated density flows in fluvio-marine setting.
(Gcs) Clast-supported conglomerate	Monomictic conglomerate in units up to 20 m thick. Clasts < 40 cm diameter, well rounded to angular in different sections. Crude stratification, imbrication common, inverse grading. Commonly rests on concave-up erosion surface.	Stream flows and concentrated debris flows in fluvio-marine setting.
(Gb) Very coarse boulder conglomerate	Monomictic conglomerate as a single bed 16.5 m thick, ~ 100 m above base of KM section, interbedded with sandstone and mudstone. Largely clast supported. Poorly sorted clasts of ultrabasic rocks < 3 m in diameter. Bedding very irregular.	Cohesive debris flow. Boulders probably originated as rock falls or landslides in valleys, transported to marine basin.
(Gc) Carbonate Conglomerate	Single, poorly stratified 9 m unit in basal conglomerates at SS section, and 3 m bed at AD section. Carbonate clasts 5-50 cm in diameter, matrix-supported, imbricated. Clasts from bedrock or intrabasinal origin.	Fluvial streamflow deposits with organized flow.
S: Sandstone		
(Sth) Thick-bedded Sandstone	Thick-bedded, medium- to very coarse-grained sandstone, with minor mudstone. Units tens of centimeters to several meters thick. Structureless, normal to inverse grading, minor cross-beds. Erosional surfaces prominent. Slumped zones. Plant and bivalve fragments, trace fossils.	Concentrated density flows to high-density turbidity flows, typically within submarine channels, near-channel sheets, and coarser lobes.
(Stb) Thin-bedded Sandstone	Thin-bedded, fine- to very fine-grained sandstone, mudstone interbeds. Sole structures, planar lamination, ripple cross-lamination, ripple-drift cross-lamination, and cross-beds common. Convolute lamination, load casts, and sand volcanoes. Plant fragments, trace fossils.	Turbidity flows, as distal overbank sheets. Deposits of levees, finer lobes, interlobe areas, and basin-floor sheets.
(Spb) Pebbly sandstone	Poorly sorted, medium- to fine-grained sandstone with scattered extrabasinal granules and pebbles. Structureless, minor cross-beds and graded beds (normal and inverse). Cross-bedded occurrences are present with the basal conglomerates of the GS section.	Concentrated or hyperconcentrated density flows, in submarine channels (Sandstone and Mudstone F.A.). Lower-regime flow in fluvio-marine channels (Basal Conglomerate F.A.).
(Smc) Mudclast sandstone	Thin (2-10 cm) beds with mud clasts up to 3 cm diameter in sandy to muddy matrix. Plant fragments common. Rest on erosional surfaces.	Erosional density flows that reworked muds, in submarine channels.
(Sc) Calclithite	Single 1 m unit, interbedded with sandstone and mudstone at 1030 m in the KM section. Thin section shows microspar, no fossil fragments noted.	Turbidity flow of reworked carbonate.
(Sd) Dolomitized calclithite	Single 10 m unit in basal part of AD section. Well bedded and highly fractured, with carbonate veins. Upper parts contain more silicate grains. Framework and veins composed predominantly of sand-size dolomitized grain. No shell fragments observed.	Orgin uncertain, possibly paleosol, or highly altered carbonate.
M: Mudstone		
(Mm) Massive mudstone	Structureless green-grey mudstones, local lamination. Calcareous concretions, 5–45 cm in diameter, near-spherical but a few discoidal. Some dark organic-rich zones.	Suspension deposits from turbidity-flow tails and hemipelagic fallout.
(Ms) Silt-rich mudstone	Rhythmic alternation of mudstone and siltstone. Siltstone in cm-scale layers, with planar lamination, ripple cross-lamination (starved formsets). Trace fossils, plant fragments.	Low-density turbidity flows and suspension settling.
C: Carbonate		
(Cm) Microspar limestone	Single 1 m unit, interbedded with sandstone and mudstone at 1030 m in the KM section. Thin section shows microspar, no fossil fragments noted.	Turbidity flow of reworked carbonate.
(Cd) Dolostone	Single 10 m unit in basal part of AD section. Well bedded and highly fractured, with carbonate veins. Upper parts contain more silicate grains. Framework and veins composed predominantly of dolomite. No shell fragments observed.	Origin uncertain, possibly paleosol, or highly altered marine or lake carbonate.

These strata are overlain by the deep-water Sandstone and Mudstone Facies Association (Poursoltani *et al.*, 2007a). Sandstone units are sheet-like with minor conglomeratic and mudstone layers. The sandstones were deposited from density flows, including turbidity currents, that traversed submarine channels and laid down sand on levees, lobes, and distal overbank areas. Separating the sandstone sheets are mudstone units tens to hundreds of metres thick (Figs. 2, 3). They are mainly grey-green with some darker beds, and contain plant fragments, ammonites, belemnites, brachiopods, and gastropods. They are interpreted as the deposits of both hemipelagic settling and low-concentration turbidity currents (Poursoltani *et al.*, 2007a). Total organic carbon varies from a mean of 0.63 wt. % in the NW of the formation to 0.27 wt. % in the SE (Karamati *et al.*, 2000). Younger mafic sills locally cut the Kashafrud Formation (Fig. 2A).

The Kashafrud Formation and the overlying carbonates and evaporites of the Upper Jurassic Mozduran Formation were followed by the deposition of the continental Shurijeh Formation during Late Jurassic to Early Cretaceous regional regression (Moussavi-Harami and Brenner, 1992).

The continental rocks are overlain by up to 4 km of marine Cretaceous strata, capped by Paleogene and Neogene continental and marine sediments with a maximum thickness of 6 km.

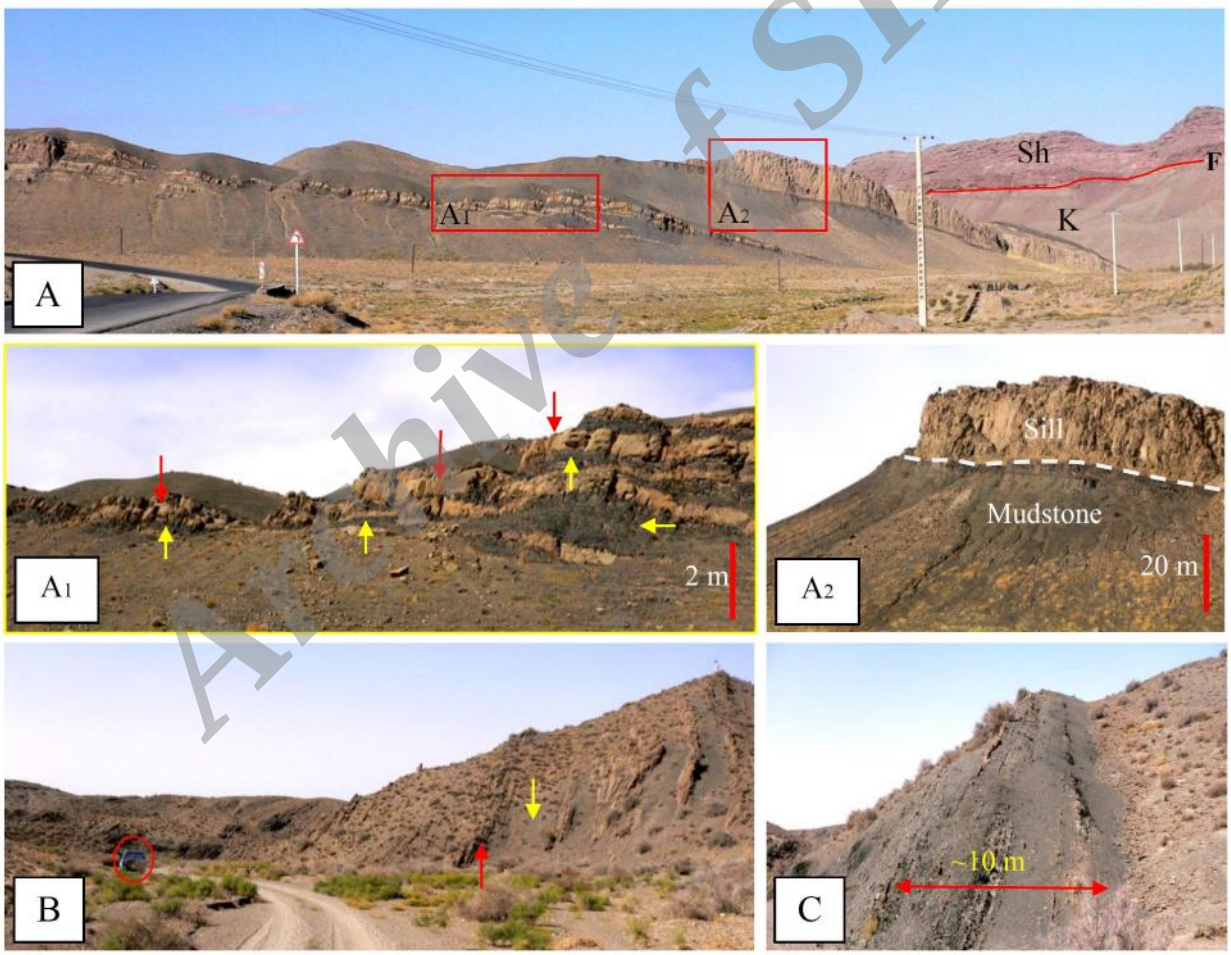

Figure 2. A) Kashafrud Formation (K), and its contact with Shourijeh Formation (Sh) in Senjedak area. Two intrusive rocks (sills) in Senjedak area are visible (red arrows showing sills, and yellow arrows showing mudstone in A1). B) Sandstone (red arrow) and mudstone packages (yellow arrow) in the Saleh-Abad section. Car for scale (red circle). C) Thick-bedded mudstone package in the Saleh-Abad section, with a package about 10 m thick visible in the distance.

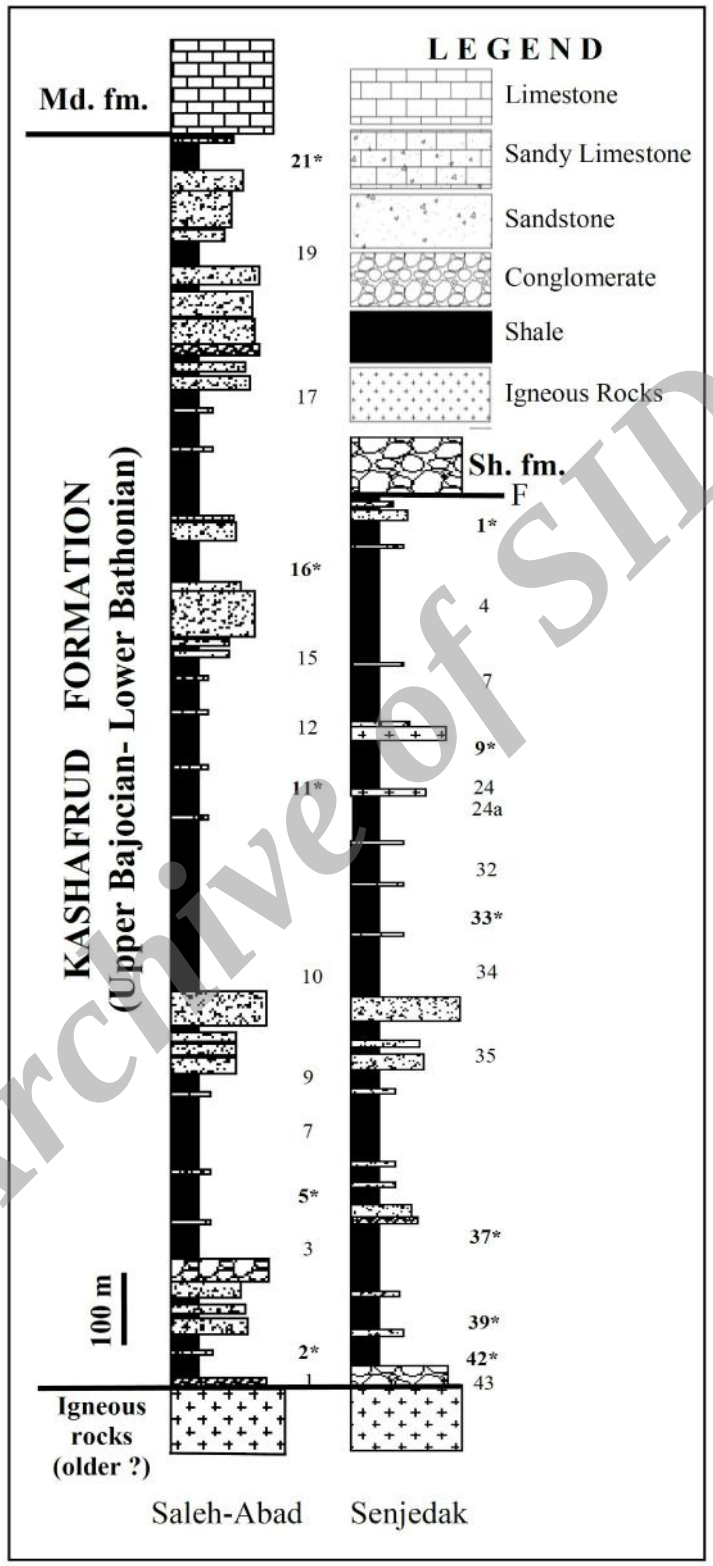

Figure 3. Summary of two measured sections showing lithofacies and sample locations. Horizontal distance is not to scale. All samples have a bulk XRD analysis. Stars showing samples with a <2 µm fraction analysis. (F: fault, Sh: Shurijeh fm., Md: Mozduran fm.)

The Kopet-Dagh Range (Fig. 1), within which the Kashafrud Formation is exposed, represents the collision zone between southern Iran and the Eurasia plate, with deformation commencing in the Miocene and continuing to the present. In northeastern Iran, this collision involved reactivation of Paleozoic and Mesozoic structures (Thomas *et al.*, 1999a, b), as well as the formation of fault-propagation anticlines above thrusts (Lyberis & Manby, 1999). The burial and exhumation history of the Kashafrud Formation is complex. Initial subsidence was followed by inversion during late Jurassic and earliest Cretaceous, after which the formation was deeply buried below late Cretaceous and early Cenozoic strata (Aghanabati, 2004). Neogene inversion created the Kopet-Dagh mountains and brought the Kashafrud strata to the surface or shallow subsurface over a wide area. A broadly comparable succession is present on the North Afghan Platform east of the study area in Afghanistan and southern Turkmenistan (Brookfield & Hashmat, 2001).

Methods

A total of 120 mudstone samples from the massive mudstone facies (Mm facies, Table 1) were collected from the outcrops of the Kashafrud Formation in the Saleh-Abad and Senjedak areas from the measured sections (Fig. 4).

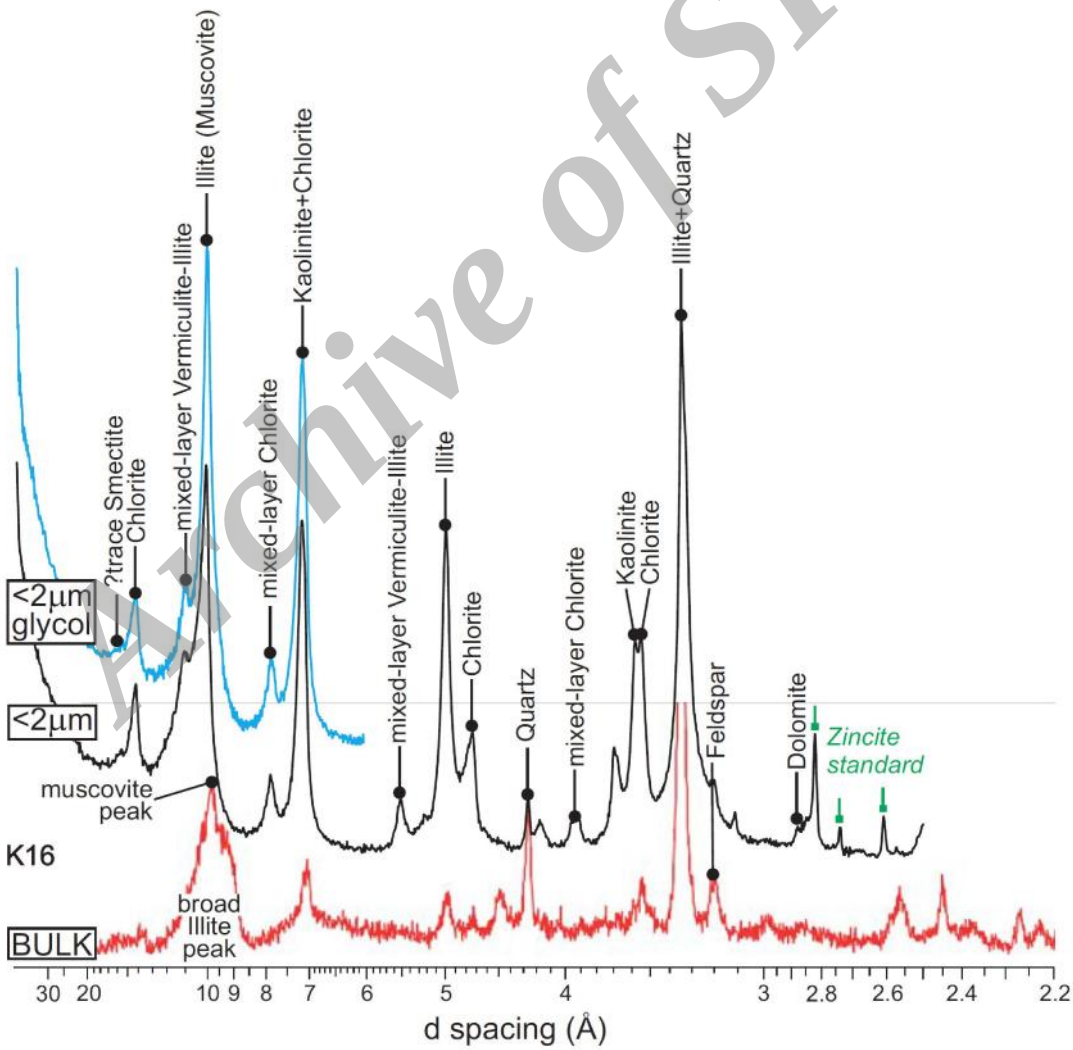

Figure 4. Typical diffractograms (sample K16) showing bulk analysis, <2 µm fraction air-dried and glycolated analyses, with identification of minerals

Detailed sedimentological and petrological context is provided by Poursoltani et al. (2007a) and Poursoltani and Gibling (2011). Mudstones are more common in Senjedak than in Saleh-Abad (Fig. 4). Clay mineral associations have been investigated using X-ray diffraction analyses on selected samples. A total of 28 bulk samples (half of which were taken from Saleh-Abad and the other half from Senjedak) were analysed using random mounts and Cu Kα radiation. From 11 of these samples the <2 µm fraction was separated, an internal standard of 5% zincite was added, and the sample analysed in oriented mounts, using a Siemens Kristaloflex diffractometer with Co Kα radiation. Air-dried samples were scanned from 2°–52° 2θ, with a 0.2° step. A shorter scan was run from 2°–17° 2θ for glycol-treated samples. The relative abundance of minerals was quantified using X-ray diffraction peak areas normalized to the zincite standard using EVA software.

The chemical composition of selected carbonates, silicates, and iron oxides was determined from the analysis and imaging of ten polished thin sections using a JEOL 8200 Superprobe model electron microprobe, with an accelerating voltage of 15 kV, beam current of 20 nA, spot size of 1 micron, and magnification of 4000x. All chemical analyses were made in the WDS (wavelength dispersive) mode.

Results

Lithofacies

Three main lithofacies are encountered in the Kashafrud Formation: 1. conglomerate; 2. sandstone; 3. mudstone, together with very minor carbonate rocks (Table 1) (Poursoltani *et al.*, 2007a). Dark gray, light gray, and greenish mudstones are the most abundant lithofacies, making up 76% of the Sandstone and Mudstone Lithofacies Association in the Senjedak section and 31.5% of the Saleh-Abad section (Fig. 2B).

The mudstones are divided into massive (Mm) and silt-rich (Ms) types, and both facies are present in all sections (Fig. 2C). They comprise mixtures of clay and silt, and are predominantly gray-green, with some black and blue-gray layers. Black mudstones, although more organic-rich than other mudstones, form diffuse layers and are not recognized here as a discrete facies. Bioturbation is visible at silt/mud contacts in the Ms facies, suggesting that other mudstones may also be bioturbated. Transported plant fossils are present in the Ms facies. Concentrations of ammonites were noted at some levels by Madani (1977) but were not observed during the present study. The mudstones are principally of turbiditic origin, but some of the Mm facies is probably hemipelagic (Madani, 1977; Poursoltani *et al.*, 2007a).

Clay minerals in the mudstones

The following minerals were identified by the X-ray diffraction of the <2 µm fraction (Fig. 4) in the approximate order of prominence of diffractogram peaks. Most of these minerals are also identified in bulk samples. Mineral identification is based on Brindley and Brown (1980) and Moore and Reynolds (1997).

Illite (-muscovite) has a [001] peak at 9.9 Å which is largely unaffected by glycolation. The peak is broad and overlaps the 11Å peak discussed below. In some bulk samples, the broad peak is clearly superimposed by a narrow peak at 9.9 Å and has corresponding secondary peaks characteristic of 2M muscovite (Fig. 4; *cf.* Verdel *et al.*, 2011). The muscovite is interpreted as detrital, and concentrated in fractions coarser than 2 µm. Kaolinite has an [001] peak at 7Å overlapping chlorite, but distinguished from chlorite by a [002] peak at 3.58Å. Chlorite has a [001] peak at 14Å, generally unaffected by glycolation (a few samples show some sharpening), a [002] peak at 7 Å that overlaps kaolinite, a [003] peak at 4.75 Å, and a [004] peak at 3.54Å. Quartz has a diagnostic peak at 4.25Å and overlaps [003] illite at 3.3 Å. Most samples show a probable mixed-layer illite-chlorite at 11Å, which appears to sharpen a little but does not shift on glycolation. In bulk samples, this forms part of the broad illite peak. A different mixed layer illite-chlorite has a clear peak at 7.8Å, unaffected by glycolation, but it is not resolved in bulk samples. In a few samples, there is a very small peak in glycolated samples at ~16Å that is absent in air-dried samples and is probably a smectite. Due to its low abundance, further characterization was not possible. There is also a reduction in peak height with glycolation in the 10.5–11.5Å range that may indicate small amounts of mixed-layer illite-smectite, but again further characterization is not possible. None of the samples have a peak above background for calcite, but dolomite is present in a few samples with a peak at 2.88 Å. In general, the X-ray diffraction of bulk samples does not reveal

the mixed layer clays, but does show a broad feldspar peak at ~3.2 Å.

Stratigraphic and geographic variations in clay mineral abundance in the mudstones

In general, less variability is seen in the <2 µm samples than in the bulk samples. The basal sample in the Saleh-Abad section (K2) is unique in lacking chlorite, mixed-layer illite-chlorite, and kaolinite (Fig. 5; Tables 2, 3). It is quite different from the basal samples (S42, S39) in the Senjedak section (Fig. 6).The occurrence of kaolinite is quite variable. Small amounts of kaolinite are difficult to detect, forming an indistinct shoulder on the 3.54Å chlorite peak. Larger amounts of kaolinite, forming a distinct peak at 3.58Å, are found only in samples K16, S1, S33, and S37. This does not seem to correlate with any other properties of the samples. The 11Å mixed-layer illite-chlorite is in general more abundant deeper in the section at both Saleh-Abad and Senjedak. The 7.8Å mixed-layer illite-chlorite is also more abundant deeper in the section (with the exception of the unusual sample at K2 which completely lacks chlorite). In general, both of these mixed layer clays are more abundant in the Saleh-Abad section than at Senjedak.

Six groups of samples are distinguished from the XRD of the bulk samples, based on the relative abundance of quartz, muscovite, illite, and undivided chlorite (± kaolinite) (Table 4):

Table 2. Relative abundance of selected minerals in bulk XRD analyses. (Abundance: 0 = not detected, 1 = trace, 2–7 ranges from small to abundant. Note that no 3.58Å kaolinite was detected.)

Sample	**height above basement (m)**	**? smectite**	**14Å-chlorite**	**muscovite**	**broad illite (mixed layer)**	**7Å-chlorite (± kaolinite)**	**quartz**	**3.54Å chlorite**	**plagioclase or muscovite**	**calcite**	**siderite**	**dolomite**
°2θ Cu Kα		*5.5*	*6.3*	*8.9*	*8.9*	*12.5*	*20.9*	*25.1*	*27.9*	*29.3*	*32.1*	*30.95*
Saleh-Abad												
17	1435	0	0	2	4	0	4	0	3	?	0	0
16	1150	2	2	2	4	3,broad	3	3	2	0	0	0
15	1040	0	2	0	4	3	3	3	3	0	0	0
12	966	1	2	2	3	3	5	2	3	2	1 ?	0
11	880	0	0	0	4	4,broad	4	3	3	2	1 ?	0
9	435	1	0	0	4	3,broad	3	3	2	3	0	0
7	370	1	0	0	4	3,broad	3	3	3	3	0	0
5	260	1	0	0	3	3	3	3	2	3	0	0
2	50	2	0	1	3	1,broad	3	1	2	0	0	2
1	2	2	?	0	2	2	7	2	3	3	0	0
Senjedak												
1	1200	2	1	3	2	3	4	2	3	0	0	0
4	1115	0	1	2	2	3	4	2	3	0	0	0
7	980	0	1	3	2	3	4	2	3	0	0	0
9	900	1	1	2	3	3	3	3	3	0	0	0
24	815	0	2	2	3	3	3	2	3	0	0	0
24A	808	0	0	3	1	2	4	2	3	0	0	0
32	710	0	1	2	1	2	4	2	3	0	0	0
33	630	2	2	2	3	3	3	2	3	1	0	0
34	560	1	2	3	1	3	4	2	2	1	0	0
35	460	0	1	2	1	3	4	2	3	0	0	0
37	200	3	1	1	3	3	4	2	3	1	0	0
39	100	1	1	2	3	3	3	3	2	1	0	0
42	20	1	3	3	2	3	3	3	2	1	0	0
43	3	2	3	2	3	4	3	3	2	4	0	0

Table 3. Relative abundance of clay minerals in the <2 µm fraction expressed as peak areas (Corg: estimated organic carbon content from colour in the field, ML: mixed layer, n.d.: not detectable, tr = trace)

Sample	height above basement	Corg	Peak height (arbitrary units)								
			16Å glyc	14Å	11Å	10Å	7.8Å	7Å	4.26Å	3.58Å	3.54Å
			?smectite	chlorite	ML vermill	illite	ML chl	chl+kaol	quartz	kaolinite	chlorite
Saleh Abad											
K2	50	low	0	tr	1800	2400	0	0	1300	0	0
K5	260	high	0	700	1120	2980	750	3900	700	tr	2700
K11	880	high	0	600	950	2700	700	3800	600	tr	2400
K16	1150	low	0	700	1150	2600	510	2400	420	1580	1600
K21	1800	low	0	550	1200	4000	550	2370	500	tr	2020
Senjedak											
S42	20	high	150	870	1750	4800	830	4130	500	0	2800
S39	100	low	0	600	1350	3600	700	3700	600	0	2280
S37	200	high	0	470	800	2370	500	2500	900	1100	1650
S33	630	low	0	500	1150	2850	400	1400	700	700	900
S9	900	SILL	0	320	730	3600	460	2010	750	0	1300
S1	1200	low	50	500	850	2560	450	2130	800	950	1300

Table 4. Different types of clay mineral assemblages from bulk XRD analyses

Type	Characteristics	Saleh-Abad	Sendejak
A	High illite, little or no chlorite	K19, K17, K2*	
B	High illite, lack of muscovite peak over a broad illite peak, moderate chlorite	K11*, K9, K7, K3	S24a
C	Broad illite with muscovite peak, moderate chlorite	K16*	S9*, S24, S37*, S39*
D	High muscovite and chlorite	K21*, K15	S43
E	Higher chlorite than illite/muscovite, high quartz	K12, K10, K5*	S7, S32, S33*, S34, S35, S42*
F	Dominant quartz	K1	S1*, S4

a) High illite, little or no chlorite
b) High illite, lack of muscovite peak over a broad illite peak, moderate chlorite
c) Broad illite with muscovite peak, moderate chlorite
d) High muscovite and chlorite
e) Higher chlorite than illite/muscovite, high quartz
f) Dominant quartz.

Types E and F are likely controlled by the grain size of the samples, with siltier samples having more quartz and chlorite.

Detrital muscovite tends to be more abundant at higher stratigraphic levels. Mg-chlorite, particularly in the <2 µm samples, appears more abundantly at deeper stratigraphic levels in both sections (Table 3, Figs. 5, 6), with the notable exception of the deepest sample in the Saleh-Abad section. Mixed-layer illite-chlorites also appear to be more abundant at deeper stratigraphic levels.

Sample S9 is within 0.5 m of the largest sill in the Senjedak section. It does not show significant differences in clay mineral assemblages compared with the other samples from the Senjedak section (Fig. 6, Tables 2, 3), except that kaolinite is either absent or present in only trace amounts. This might be due to the local thermal effect of the sill, since laboratory heating to >550 °C causes the kaolinite structure to collapse. However, other samples such as K5 and K11 have no detectable kaolinite, so the lack of kaolinite might be related to supply.

Diagenetic minerals in sandstones

Study of the paragenetic sequence of diagenetic minerals in sandstones interbedded with the mudstones may provide some constraints on the diagenetic changes in mudstones. SEM backscattered electron images show eogenetic pore-filling kaolinite in small amounts, particularly in the Saleh-Abad section, but no other diagenetic minerals clearly postdate this kaolinite and predate quartz overgrowths.

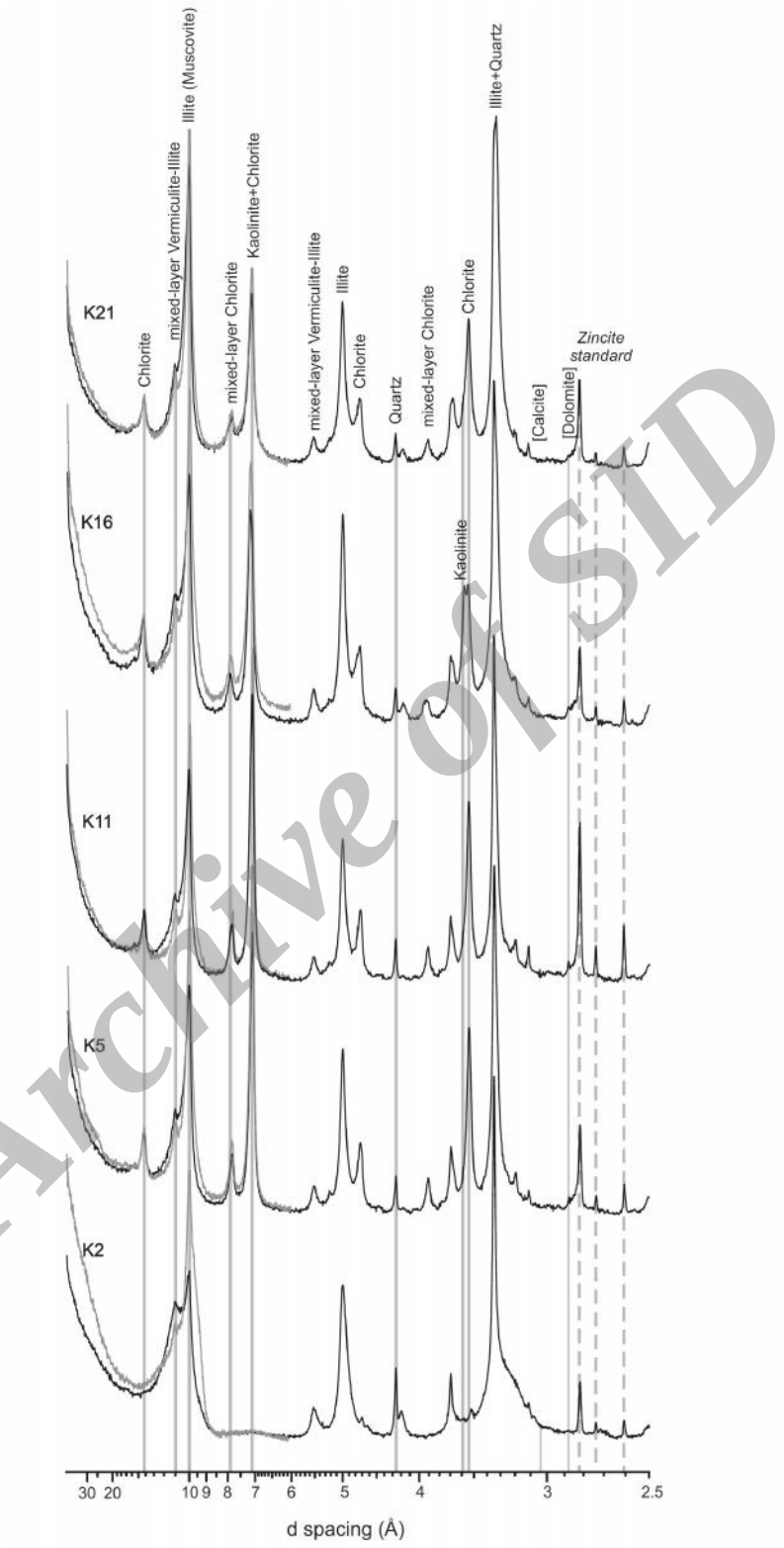

Figure 5. Stratigraphic variation in clay minerals in the Saleh-Abad section, shown by stacked X-ray diffractograms of the <2 µm fraction (Black: air dried, grey: glycolated)

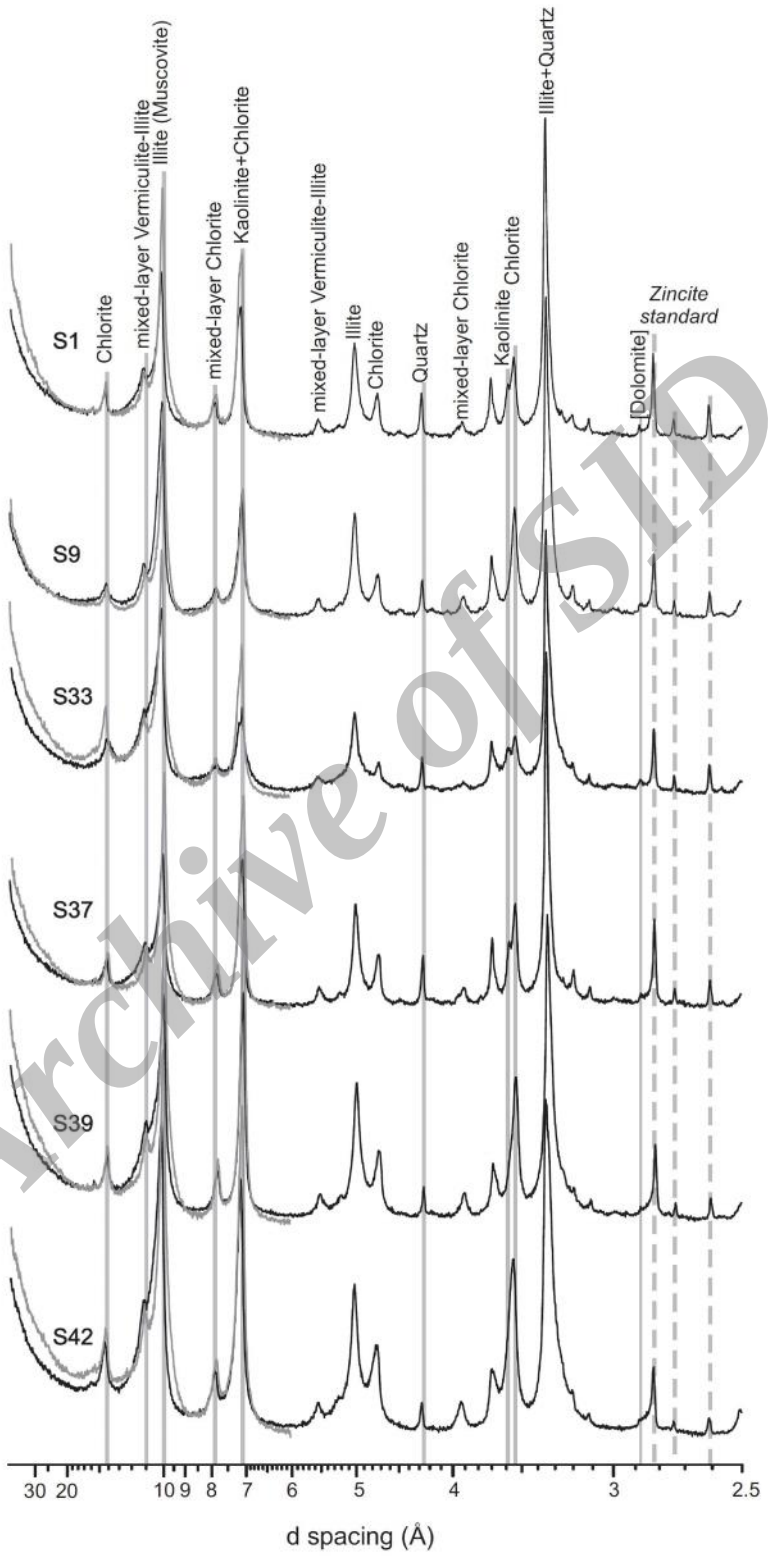

Figure 6. Stratigraphic variation in clay minerals in the Senjedak section, shown by stacked X-ray diffractograms <2 µm fraction (Black: air dried, grey: glycolated)

Mesogenetic chlorite is present in both studied sections, as chlorite rims and as fibrous pore-filling chlorite. Some chlorite rims are formed around detrital grains of quartz and overlie Fe-rich clays (Fig. 7A). Chlorite + illite is common in pores adjacent to altered K-feldspar. Nowhere does pore-filling chlorite + illite clearly postdate quartz overgrowths, but it predates widespread carbonate cementation in Kashafrud Formation sandstones (Fig. 7B). The carbonate cements include ferroan calcite, ankerite and siderite (Fig. 7C). In our study, no morphological evidence for chloritization of kaolinite has been seen. Kaolinite cement is engulfed by later barite and illite (Fig. 7D).

Discussion

Relationship of clay minerals to vitrinite reflectance

No consensus has been reached among previous authors (Afshar Harb, 1979; Poursoltani & Gibling, 2011) on the degree of the diagenesis of the sediments and organic matter of the Kashafrud Formation. Thickness estimates of overlying strata in the literature are maxima, and the Kashafrud Formation may originally have been overlain by about 5 km of strata in the study area, although this estimate is poorly constrained. The Kashafrud Formation, from 450 to 1500 m above its base, yielded vitrinite reflectance values of 0.64–0.83% (Table 5), rated as early mature to mature, in the oil window (Heroux *et al.*, 1979; Mukhopadhyay, 1992; Poursoltani & Gibling, 2011). This measured vitrinite reflectance in the Kashafrud Formation is consistent with burial to 2–3 km (Corcoran and Clayton, 2001). At these vitrinite reflectance values, mixed-layer smectite-illite is common in other basins (e.g. Sachsenhofer *et al.*, 1998; Abid & Hesse, 2007).

The sills in the Senjedak section (Fig. 2A) have no pronounced effect on the adjacent clay minerals, suggesting that the entire basin was affected by relatively high geothermal gradient during sill emplacement. That geothermal gradient, based on total stratigraphic thicknesses, was likely >100 °C/km, but may not have been of long duration.

Burial history of cements in sandstones

The burial history of the sandstones interbedded with the mudstones may provide some constraints on the evolution of clay minerals in the mudstones. In both the study areas, early kaolinite is found in small amounts in sandstones, perhaps implying that even fully marine facies experienced some flux of meteoric water, as noted elsewhere by Karim *et al.* (2010). Mesogenetic chlorite rims probably formed by the transformation of berthierine to chlorite, which occurs at temperatures greater than 70-100ºC (e.g. Aagaard *et al.*, 2000; Worden and Morad, 2003). Late diagenetic pore-filling minerals are calcite and ankerite, with lesser illite and chlorite + illite. Ankerite and illite are normally characteristic of temperatures >120 ºC (Morad *et al.*, 1990; Hendry *et al.*, 2000; Worden & Morad, 2003).

Table 5. Vitrinite reflectance from the Kashafrud Formation. (Modified from Poursoltani and Gibling, 2011)

Sample	Meters above formation base	%Ro of autochthonous grains (mean %)	Std. Dev.	Comments	Autochthonous vitrinite grains/total measured	Ro of all grains (mean %)
9	1500	0.83	0.06	Mature	8/15	0.97
8	1150	0.74	0.08	Mature	8/18	1.22
7	1100	0.67	0.09	Early Mature	18/33	0.89
6	1000	0.64	0.06	Early Mature	20/50	0.84
5	630	0.69	0.11	Mature	7/11	0.99
4	450	0.73	0.06	Mature	9/28	1.07
3	130	2.59	0	Oxidized	1/13	3.13
2	70	2.09	0.13	Partially oxidized	20/50	2.2
Coal	Triassic	2.22	0.11	Overmature	47/50	2.16

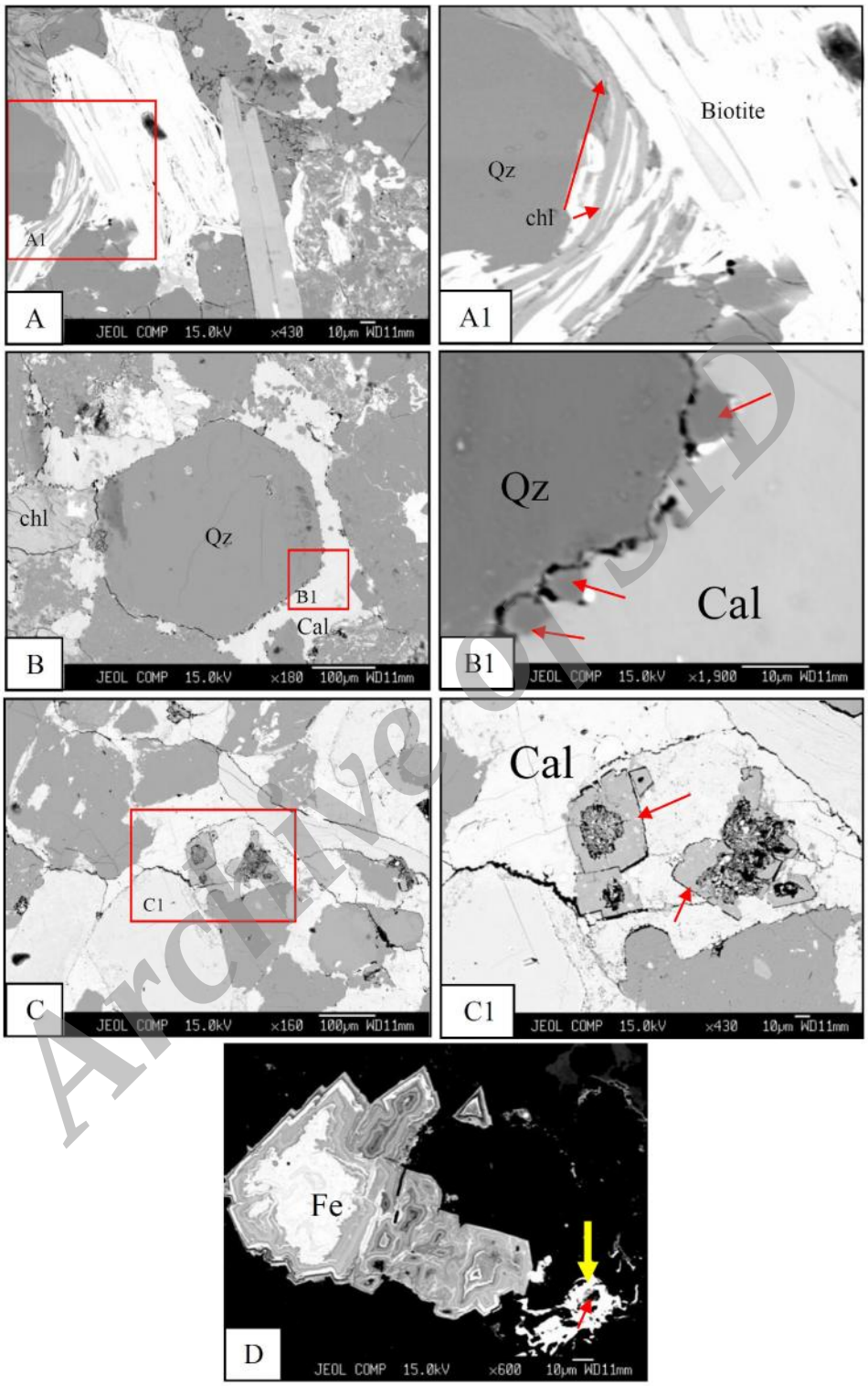

Fig. 7. Back-scattered electron images showing some of the different types of the diagenetic minerals present in two sandstones from the study area. A) chlorite (chl) rims around a detrital grain (Qz); B) chlorite rims postdate quartz overgrowth (arrows), but predate widespread carbonate cementation (Cal); C) microcrystalline diagenetic siderite (arrows), D) pore-filling iron oxide (Fe) and diagenetic barite (yellow arrow), and diagenetic kaolinite (red arrow).

This is consistent with temperatures estimated from vitrinite reflectance at intervals where ankerite is abundant in the Kashafrud Formation (Poursoltani and Gibling, 2011). However, in the overlying Mozduran Formation limestones, maximum mperature of carbonate cement formation was estimated as 50 º C (Mahboubi *et al.*, 2010).

Role of the burial diagenesis of clay minerals in mudstones

Stratigraphic variation in most clay minerals appears at random, suggesting that variation in illite, smectite, and kaolinite is due more to changes in source or grain size than to progressive changes during burial diagenesis. Chlorite is more abundant in deeply buried mudstones. Peak heights for 7.8Å mixed-layer illite-chlorite and 11Å mixed-layer illite-chlorite tends to increase with burial depth and probably reflects increasing order and crystallinity with depth.

The paucity of smectite might be because it was not supplied to the basin, or because it has been converted to illite by deep burial diagenesis. Elsewhere, conversion of smectite to illite has been observed at burial depths of 1.5 to 3.5 km (Aoyagi and Kazama, 1980; Chamley, 1989; Velde, 1995; El Albani *et al.*, 2002), which is the likely range of the burial depth of the Kashafrud Formation based on stratigraphic evidence and the vitrinite reflectance discussed above. The evidence of little or no illite-smectite mixed layer clays in the Kashafrud Formation suggests that the paucity of smectite is probably not due to illitization, but due to low original supply.

Probable detrital sources of clay minerals in mudstone units

The abundance of poorly crystalline illite may indicate an important source from pre-existing illitic mudstones. Some samples seem to have an important crystalline metamorphic source with high muscovite and chlorite (*e.g.*, K21, K15, Fig. 8). Others have predominant illite of relatively low crystallinity, presumably from older illitic mudstones, with little or no muscovite or chlorite (*e.g.*, K19, K17, K2, Fig. 8). Still other samples seem to be a mixture between the two sources. The crystalline metamorphic source tends to be more important at higher stratigraphic levels, suggesting the progressive unroofing of crystalline basement. The abundance of kaolinite does not appear to correlate with the supply of feldspar (Tables 2, 3; Fig. 8).

Detrital minerals within sandstones of the Kashafrud Formation provide some clues as to the sources of clay minerals. In sandstones, detrital muscovite and K-feldspar are common and have altered to kaolinite. The abundant K-feldspar, despite the warm paleoclimate (Mahboubi *et al.*, 2010), suggests the rapid unroofing of granitoid source areas. In mudstones, well-crystallised muscovite and chlorite suggest active erosion of crystalline metamorphic bedrock. The metamorphic basement and granitoid plustons were exposed and eroded during the collision of Paleotethys and the opening of Neotethys (Golonka, 2004; Lyberis and Manby, 1999; Thomas *et al.*, 1999a, b; Poursoltani *et al.*, 2007a, b).

The distinction between diagenetic and detrital clay minerals

There may be a continuum between detrital and diagenetic clay minerals, as original detrital minerals recrystallize during burial. The co-existence of well-crystallized muscovite and poorly crystallized illite over all ranges of depth is difficult to account for by diagenetic processes and suggests that both are detrital. The lack of correlation of either smectite or kaolinite with burial depth, and the lack of illite-smectite mixed-layer clays despite the burial conditions being suitable, suggest that the kaolinite and smectite are also predominantly detrital. Assigning an origin to the chlorite is more difficult, as a variety of chlorite types may be present. The low height of the [001] and [003] peaks compared to the [004] suggests that much of the chlorite is Mg-rich and thus more likely to be of detrital origin, as diagenetic chlorite is predominantly Fe-rich (Ryan & Hillier, 2002). On the other hand, the abundance and crystallinity of mixed-layer illite-chlorite increases with burial depth and this is a typical diagenetic mineral in sedimentary basins.

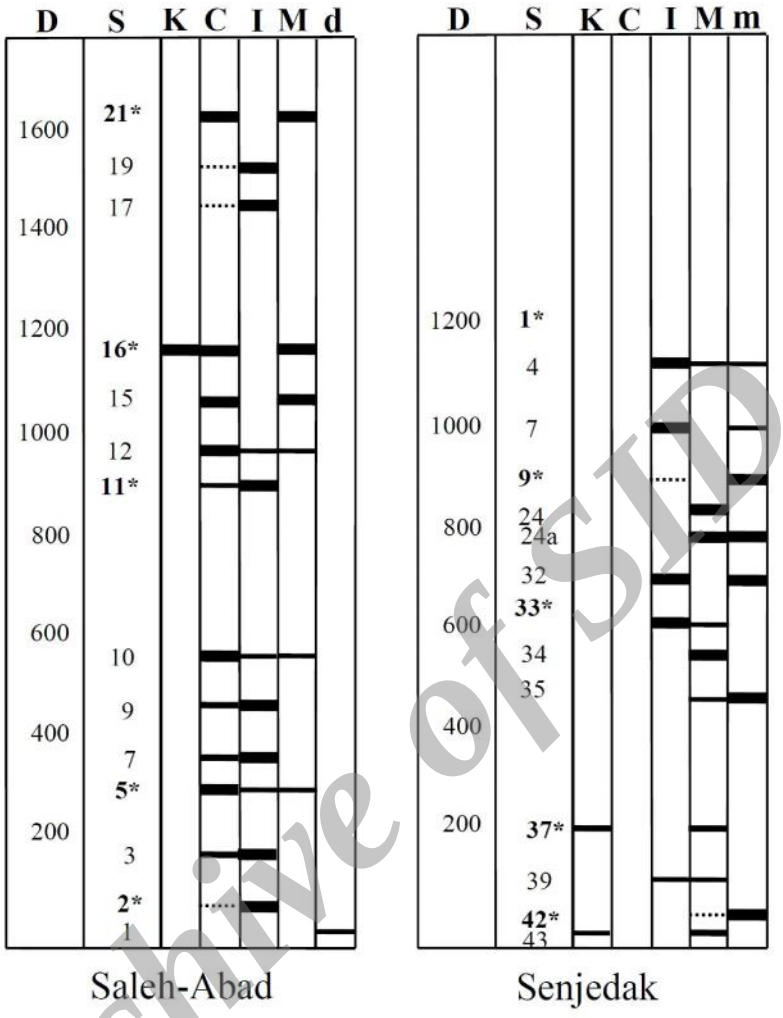

Figure 8. Relative abundance of clay minerals by stratigraphic position in two measured sections. Heavy lines represent major clay minerals, light lines represent minor clay minerals, and dashed lines represent probable clay minerals. (D: depth/m, S: sample, C: chlorite, I: illite, K: kaolinite, M: muscovite, m: mixed layer clays, d: dolomite)

Conclusions

1. Mudstones in the Kashafrud Formation contain illite, muscovite, mixed layer illite-chlorite and chlorite. Some samples contain kaolinite or very minor smectite.

2. Mixed-layer illite-chlorite become more ordered and crystallized with depth; chlorite also increases in abundance or crystallinity with depth. Burial diagenesis probably took place at depths of 2–3 km. There is no evidence either for a significant supply of smectite nor for the diagenetic alteration of smectite to illite.

3. Two sources of illite are distinguished: illitic mudstones and crystalline basement, the latter also supplying detrital muscovite and chlorite. The crystalline basement source was more important at higher stratigraphic levels, suggesting the progressive unroofing of the hinterland. The source area was rapidly uplifted, as suggested by the abundance of K-feldspar in the sandstones despite the warm paleoclimate.

4. Igneous sills in the Senjedak section have no pronounced effect on adjacent clay minerals, suggesting that the entire basin was affected by relatively high geothermal gradient during sill emplacement.

Acknowledgements

The authors would like to thank the journal reviewers for their thoughtful and constructive comments which greatly improved the manuscript. We also acknowledge support from the Islamic

Azad University of Mashhad, Iran. Work by GPP was supported by a Natural Sciences and Engineering Research Council of Canada Discovery Grant.

References

Aagaard, P., Jahren, J., Harstad, A.O., Nilsen, O., Ramm, M., 2000. Formation of grain coating chlorite in sandstones; laboratory synthesized vs. natural occurrences. Clay Minerals. 35: 261-269.

Abid, I., Hesse, R., 2007. Illitizing fluids as precursors of hydrocarbon migration along transfer and boundary faults of the Jeanne d'Arc Basin offshore Newfoundland, Canada. Marine and Petroleum Geology. 24; 237-245.

Afshar-Harb, A., 1979. The Stratigraphy, Tectonics and Petroleum Geology of the Kopet Dagh Region, Northern Iran, Ph.D. thesis, Imperial College of Science and Technology, University of London, London, England, 316 pp.

Aghanabati, A., 2004. Geology of Iran. Geological Survey of Iran Publication, 586 pp. (in Persian).

Aoyagi, K., Kazama, T., 1980. Transformational changes of clay minerals, zeolites and silica minerals during diagenesis. Sedimentology. 27: 179-188.

Brindley, G.W., Brown, G., 1980. Crystal Structures of Clay Minerals and their X-ray Identification. Mineralogical Society, London, 495 pp.

Brookfield, M.E., Hashmat, A., 2001. The geology and petroleum potential of the Norte Afghan platform and adjacent areas (northern Afghanistan, with parts of southern Turkmenistan, Uzbekistan and Tajikestan). Earth-Science Reviews. 55: 41-71

Chamley, H., 1989. Clay Sedimentology. Springer, Berlin. 623 pp.

Corcoran, D.V., Clayton, G., 2001. Interpretation of vitrinite reflectance profiles in sedimentary basins, onshore and offshore Ireland. Geological Society, London, Special Publications. 188: 61-90.

Eftekhar-Nejad, J., Alavi-Naini, M., Behrouzi, A., 1993. Geological map of Torbate- Jam, scale 1: 250,000 (one sheet), Geological Survey of Iran.

El Albani, A., Cloutier, R., Candilier, A.M., 2002. Early diagenesis of the Upper Devonian Escuminac Formation in the Gaspé Peninsula, Québec: sedimentological and geochemical evidence. Sedimentary Geology. 146: 209-223.

Ghaemi, F., 2004. Geological map of Agh-Darband, scale 1: 100,000 (one sheet), Geological Survey of Iran.

Golonka, J., 2004. Plate tectonic evolution of the southern margin of Eurasia in the Mesozoic and Cenozoic. Tectonophysics. 381: 235-273.

Hendry, J.P., Wilkinson, M., Fallick, A.E., Trewin, N.H., 2000. Dissiminated 'jigsaw-piece' dolomite in Upper Jurassic shelf sandstones, Central North Sea: an example of cement growth during bioturbation?, Sedimentology. 47: 631-644.

Heroux, Y., Chagnon, A., Bertrand, R., 1979. Compilation and correlation of major thermal maturation indicators, American Association of Petroleum Geologists, Bulletin. 63: 2128-2144.

Karamati, M., Tavallai, M., Angaji, M., Memariani, M., 2000. Hydrocarbon potential and migration system of Kashafroud Formation, in Kopet Dagh sedimentary basin, NE Iran. 16th World Petroleum Congress, 11-15 June, Calgary, Canada. https://www.onepetro.org/conference-paper/WPC-30121

Karim, A., Pe-Piper, G., Piper, D.J.W., 2010. Controls on diagenesis of Lower Cretaceous reservoir sandstones in the western Sable Subbasin, offshore Nova Scotia. Sedimentary Geology. 224: 65-83.

Kavoosi, M.A., Lasemi, Y., Sherkati, S., Moussavi-Harami, R., 2009. Facies analysis and depositional sequences of the Upper Jurassic Mozduran Formation, a carbonate reservoir in the Kopet Dagh Basin, NE Iran. Journal of Petroleum Geology. 32: 235-260.

Lasemi, Y., 1995. Platform carbonates of the Upper Jurassic Mozduran Formation in the Kopet Dagh Basin, NE Iran-facies paleoenvironments and sequences. Sedimentary Geology. 99: 151-164.

Lyberis, N., Manby, G., 1999. Oblique to orthogonal convergence across the Turan Block in the post-Miocene. American Association of Petroleum Geology Bulletin. 83: 1135-1160.

Mahboubi, A., Moussavi-Harami, R., Carpenter, S.J., Aghaei, A., Collins, L.B., 2010. Petrographical and geochemical evidences for paragenetic sequence interpretation of diagenesis in mixed siliciclastic–carbonate sediments: Mozduran Formation (Upper Jurassic), south of Agh-Darband, NE Iran. Carbonates Evaporites. 25: 231-246.

Madani, M., 1977. A study of the sedimentology, stratigraphy and regional geology of the Jurassic rocks of eastern Kopet Dagh (NE Iran), Ph.D. thesis, Royal School of Mines, Imperial College, London, England, 246 pp.

Moore, D.M., Reynolds, Jr, R.C., 1997. X-ray diffraction and the identification and analysis of clay minerals. Oxford University Press, New York. 378 pp.

Morad, S., Bergan, M., Knarud, R., Nystueu, J.P., 1990. Albitization of detrital plagioclase in Triassic reservoir sandstone from the Snorre Field, Norwegian North Sea. Journal of Sedimentary Petrology. 60: 411-425.

Moussavi-Harami, R., Brenner, R.L., 1992. Geohistory analysis and petroleum reservoir characteristics of Lower Cretaceous (Neocomian) sandstones, eastern Kopet Dagh Basin, northeastern Iran. American Association of Petroleum Geology Bulletin. 76: 1200-1208.

Mukhopadhyay, P.K., 1992. Maturation of organic matter as revealed by microscopic methods: applications and limitations of vitrinite reflectance, and continuous spectral and pulsed laser fluorescence spectroscopy. In: Wolf KH, Chilingarian GV, (Eds.), Diagenesis, III. Developments in Sedimentology, Elsevier, New York. 47: 435-510.

Poursoltani, M.R., Moussavi-Harami, R., Gibling, M.R., 2007a. Jurassic deep-water fans in the Neo-Tethys Ocean: The Kashafrud Formation of the Kopet-Dagh Basin, Iran. Sedimentary Geology. 198: 53-74.

Poursoltani, M.R., Moussavi-Harami, R., Lasemi, Y., 2007b. Environmental interpretation of Kashafrud Formation (Upper Bajocian-Lower Bathonian) based on ichnofossils, NE Iran. Geosciences. 65: 170-185. (in Persian, abstract in English).

Poursoltani, M.R., Gibling, M.R., 2011. Composition, porosity and reservoir potential of the Middle Jurassic Kashafrud Formation northeast Iran. Marine and Petroleum Geology. 28: 1094-1110.

Poursoltani, M.R., Kargar, M., 2012. Analysis of Middle Jurassic coarse grain deposits, in the East of Kopet-Dagh Basin, Iran. Sedimentary Facies. 4: 135-150 (in Persian, abstract in English).

Ryan, P. C., Hillier, S., 2002. Berthierine/chamosite, corrensite, and discrete chlorite from evolved verdine and evaporite-associated facies in the Jurassic Sundance Formation, Wyoming: American Mineralogist, 87: 1607–1615.

Sachsenhofer, R.F., Rantitsch, G., Hasenhüttl, C., Russegger, B., Jelen, B., 1998. Smectite to illite diagenesis in early Miocene sediments from the hyperthermal western Pannonian Basin. Clay Minerals. 33: 523-537.

Taheri, J., Fursich, F.T., Wilmsen, M., 2009. Stratigraphy, depositional environments and geodynamic significance of the Upper Bajocian-Bathonian Kashafrud Formation, NE Iran, in: Brunet, M.-F., Wilmsen, M., Granath, J.W. (Eds.), South Caspian to Central Iran Basins, London, UK, Geological Society Special Publication. 312: 205-218.

Thomas, J.C., Cobbold, P.R., Shein, V.S., Le Douaran, S., 1999a. Sedimentary record of late Paleozoic to Recent tectonism in central Asia—analysis of subsurface data from the Turan and south Kazak domains. Tectonophysics. 313: 243-263.

Thomas, J.C., Grasso, J.R., Bossu, R., Martinod, J., Nurtaev, B., 1999b. Recent deformation in the Turan and South Kazakh platforms, western central Asia, and its relation to Arabia–Asia and India–Asia collisions. Tectonics. 18: 201-214.

Velde, B., 1995. Origin and Mineralogy of Clays: Clays and the Environment. Springer, Berlin, pp. 234-240.

Verdel, C., Niemi, N., van der Pluijm, B.A., 2011. Variations in the illite to muscovite transition related to metamorphic conditions and detrital muscovite content: insight from the Paleozoic passive margin of the southwestern United States. Journal of Geology. 119: 419-437.

Worden, R.H., Morad. S., 2003. Clay minerals in sandstones: a review of the detrital and diagenetic sources and evolution during burial. In: Worden, R.H., Morad, S. (Eds.), Clay cement in sandstones, International Association of Sedimentologists, Special Publication, 34: 3-41.